# A Theoretical Study of Cyclic Pyrene Oligomers and Their Resemblance with Cyclic Paraphenylenes: Disclosing Structure-Property Relationships for Cyclic Nanorings

M. Moral, A. Pérez-Guardiola, E. San-Fabián, A. J. Pérez-Jiménez, J.C. Sancho-García.*

Departamento de Química Física, Universidad de Alicante, E-03080, Alicante, Spain.

* E-mail: jc.sancho@ua.es; telephone: +34/965903536

## ABSTRACT

We theoretically discuss here the relationships between the structure of recently synthesized nanorings, dubbed as cyclo-2,7-pyrenylene (CPY) and formed upon bending and bonding a finite number of pyrene units until self-cyclation, and a set of chemically relevant properties such as the induced structural and energetical strain, the electronic and optical properties, or the response to charge injection, as well as their transport mechanism through a concerted migration of charge-carriers. We also compare these properties, and their evolution with the number of pyrene-linked units, with those obtained for the closely related cycloparaphenylene (CPP) compounds, trying to disclose the underlying structure-property guidelines. To do it, we always employ dispersion-corrected DFT methods to systematically include the key effects affecting all the properties tackled. A correct match with some available experimental results, for the [4]CPY compound (the only one synthesized so far), anticipates the accuracy of the calculations done for the rest of compounds. Finally, since this kind of systems are envisioned as possible precursors for the fine-tuned and controlled synthesis of carbon nanotubes, we also address the stability of the dimers found in their crystalline structure, and the associated cohesive energy, which may drive the synthesis of the corresponding nanotubes after an adequate dehydrogenation reaction.

## INTRODUCTION

Cyclic and conjugated organic structures, such as carbon nanotubes and nanorings,[1] comprise a wide variety of interesting examples of strained, distorted, bent and sterically hindered molecular systems. Furthermore, besides the large interest in their unique chemical bonding, formed only by $sp^2$ hybridized carbon atoms, these structures have been widely studied due to their interesting physical, chemical, and electronic properties, taken also into account how these properties can be modulated as a function of their molecular size, shape and crystallinity.[2] In the last years, many studies focused on a kind of cyclic organic molecules called cycloparaphenylenes (CPP) (see figure 1), which are obtained by connecting phenyl rings through *para* linkages until forming a cyclic nanohoop. Thus, several sizes of CPPs (ranging from [5]CPP to [18]CPP or even higher, where the number in brackets indicates the phenyl rings attached), as well as CPP derivatives and related carbon nanorings, have been recently synthetized,[3,4] and their structural and electronic properties largely studied.[5] However, there are very few studies about acene-inserted CPPs, in which the acene structures can be polycyclic aromatic hydrocarbons (such as naphthalene,[6] pyrene, [7-9] chrysene[10] or anthanthrylene[11] moeties), annulated derivatives,[12,13] or heteroacenes (such as pyridine,[14,15] thiophene,[16,17] anthraquinone,[18] carbazole[19] and perylene diimide[20]) in addition to benzene rings. The systematic study of these structures could allow the elucidation of the structural and electronic effects present in the carbon nanorings composed by more π-extended systems.

In this work, we have thus focused on a set of acene-inserted CPPs, formed upon progressively bending pyrenylene units to form a cyclic hoop called Ciclo-2,7-PYrenylene (CPYs) structures, which are related to the armchair structure of the carbon nanotubes (CNTs) (see figure 1). The study of these systems can clarify some interesting properties derived from more π-extended systems such as a higher structural strain, chiral conformations, size-evolution of properties, etc. Furthermore, despite of some similarity between pyrene and biphenyl rings, their structural and electronic structure are completely different, motivating us to study the effect of inserting pyrene units inside these cyclic organic structures.[21] In this sense, the comparison between CPY and CPP analogues could be useful to understand their behavior as precursors for the bottom-up synthesis of structurally uniform armchair CNTs, or for some other envisioned applications of these promising CNT segments.[22]

Herein, we have studied from a theoretical point of view a series of CPYs (ranging between [3] to [5]CPYs) in order to determine: (i) how the structural, electronic, and energetical properties of isolated [3-5]CPY systems theoretically evolve with system size; and (ii) how these systems self-assemble in the solid-state, chosen [4]CPY (the only system synthesized so far) as a case study, after calculating the non-covalent interactions between the set of unique molecular arrangements found in crystalline samples. Moreover, taking account that pyrene is a substituent of large interest in many opto-electronic applications,[23] the charge injection and transport properties of solid-state samples of [4]CPY have been subsequently modelled. In the next sections, we will thus present and discuss the key properties of [3-5]CPY individual (gas-phase) molecules, and the supramolecular interaction energy as well as the charge-transport features of [4]CPY, thoroughly comparing these properties, at the same level of theory, with the [2n]CPP parent compounds (see also figure 1) in an attempt to establish structure-property relationships.

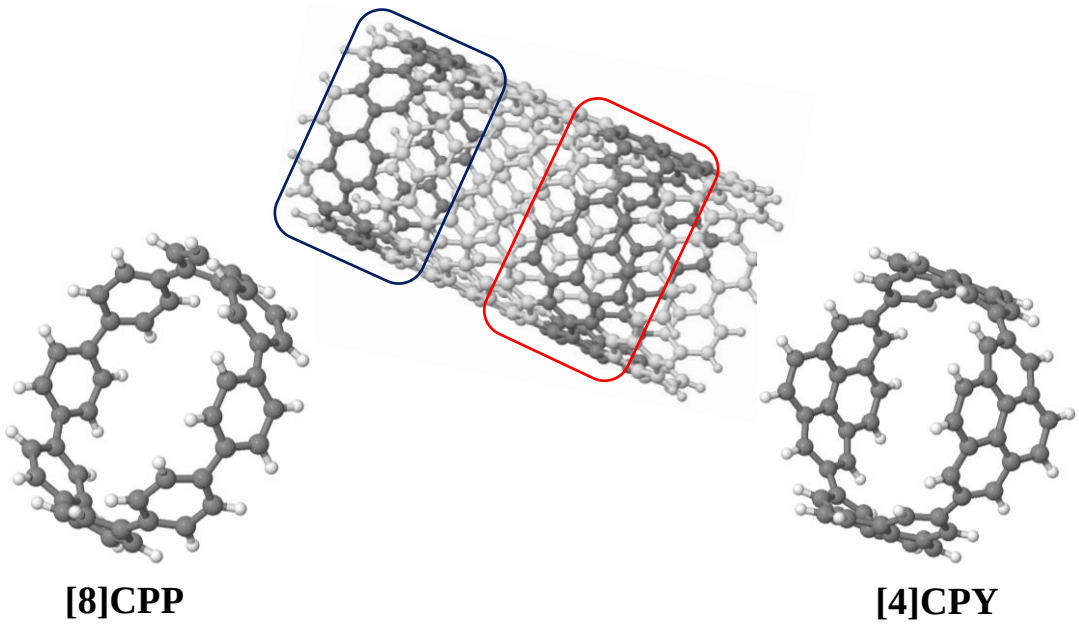


**Figure 1**. Sketch of a nanotube structure from which it would be possible to extract segments such as [8]CPP and the more π-extended structure [4]CPY.

## COMPUTATIONAL DETAILS

The Gaussian09 package (Rev. D.01)[24] has been employed for all the calculations performed here, except for electronic coupling ($V_{if}$) values (vide infra), which have been obtained using the NWChem 6.5 package thanks to the charge transfer module implemented on it.[25] Density Functional Theory (DFT) with the hybrid functional B3LYP[26,27] was employed, together with the Pople's (6-31+G*) and Dunning's (cc-pVnZ) basis sets for the computation of the electronic, geometrical, energetical and supramolecular properties of the studied CPYs. We have chosen the B3LYP model since it yields reasonable conjugated-polymer ground-state structures,[28,29] and, in general, is appropriate for the prediction of electronic structures of polycyclic aromatic hydrocarbons.[30] In addition, that method provides theoretical reorganization energies ($\lambda_i$) in good quantitative agreement with the corresponding experimental values from gas phase ultraviolet photoelectron spectroscopy.[31]

These studies were carried out taking also into account all the existing non-covalent (intra- and intermolecular) interactions, by incorporating the correction known as D3(BJ)[32,33] to the hybrid functional mentioned above. This way of considering the non-covalent energy has revealed to be an efficient and accurate method.[34] On the other hand, the use of the sufficiently large cc-pVTZ basis set allows us to greatly reduce the associated Basis Set Superposition Error (BSSE) in supramolecular calculations.

One-electron properties (such as frontier energy orbitals, ionization potentials and electron affinities) were calculated on optimized CPY structures, unless otherwise specified. Closed-shell calculations for singlets and open-shell calculations for doublets (cationic and anionic species) have been carried out for the different derivatives [3-5]CPY. $V_{if}$ calculations were carried out over each [4]CPY dimer extracted from the crystalline structure, by using the UHF/cc-pVDZ level of theory.

Finally, considering excited-state calculations, the time dependent (TD)-DFT formalism[35] has been used, together with the PBE0[36] hybrid functional and the cc-pVDZ basis set, to disclose the nature of the UV-Vis absorption,

through electronic transitions with high oscillator strength values (*f*) involving frontier MOs extended along the whole system.

## RESULTS AND DISCUSSION

**Properties of isolated [n]CPY nanorings.** The structures of the neutral and charged [n]CPY systems have been optimized at the B3LYP-D3(BJ)/cc-pVDZ level, without symmetry constraints but carefully checking that all the frequencies were positive in all cases. We have further analyzed the structural parameters (i.e., diameter of the inner cavity of the nanoring and bond length between *ipso* and *ortho* carbons, see figure 2), strain energies and absorption wavelengths of the studied [n]CPYs. The diameter has been estimated as the distance between the opposite *ipso* carbon atoms for the even-numbered member or as the distance between the *ipso* carbon atom and the center of mass of the opposite pyrene ring for the odd-numbered members. As we expected (see table 1), the diameter of the [n]CPY systems increases with the number of pyrene rings into the structure, with only slight differences between the neutral and the charged structures. This difference for anionic structures ranges from 0.006 to 0.124 Å, while for cationic structure, the value situates between 0.022 – 0.090 Å. Moreover, comparing the diameter of [n]CPY with their analogous [2n]CPP nanorings,[37] the values for the latter are slightly lower than those of the corresponding [n]CPY, with a decrease of 0.04 and 0.10 Å for [4]CPY and [3,5]CPY, respectively.

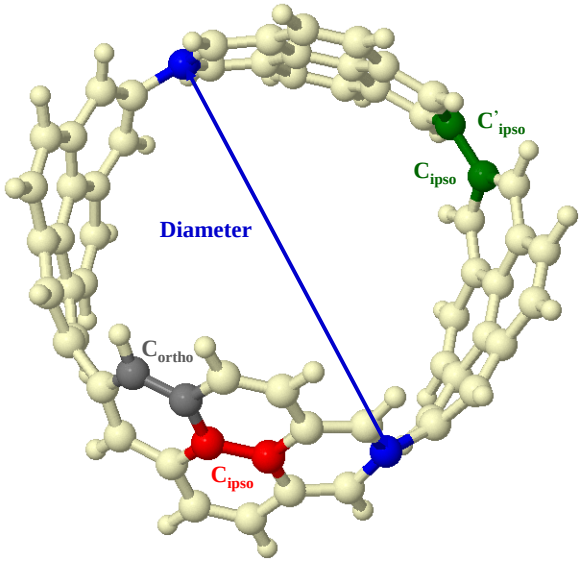


**Figure 2.** Sketch of [4]CPY where $C_{ortho}$ and intra-ring (inter-ring) $C_{ipso}$ are shown in marked grey and red (green) colors, respectively; the diameter of the nanohoop is also displayed.

With respect to some key bond lengths (see table 1), we have not found striking differences in the distance of $C_{ipso}$-$C_{ortho}$, $C_{ipso}$-$C_{ipso}$, $C_{ortho}$-$C_{ortho}$ among the neutral [n]CPYs, which indicates that the near-planarity and conjugation of these systems remains similar, regardless of their size. For charged (anionic and cationic) structures, the distance between $C_{ipso}$-$C_{ortho}$ decreases slightly with the increasing number of pyrene rings, observing the opposite behavior for the $C_{ipso}$-$C_{ipso}$ distance. However, for the $C_{ortho}$-$C_{ortho}$ bond length, we have not found significant differences for the studied (neutral or charged) [n]CPY structures. Furthermore, the distance between $C_{ipso}$-$C'_{ipso}$, is close to 1.50 Å in all cases, prevailing thus a single-bond character between the pyrene units. Note also that these calculated distances, for

the case of the neutral [4]CPY are within 0.01 – 0.02 Å with respect to the available X-Ray results,[20] also indicating weak intra-molecular structural distortions upon crystallization.

**Table 1**. **Diameter (d, in Å) and selected bond lengths (R, in Å) of [n]CPY structures, in their neutral, anionic, and cationic forms, calculated at the B3LYP-D3(BJ)/cc-pVDZ level.**

| | [3]CPY | | | [4]CPY | | | [5]CPY | | |
|---|---|---|---|---|---|---|---|---|---|
| | Neutral | Anionic | Cationic | Neutral | Anionic | Cationic | Neutral | Anionic | Cationic |
| Diameter (d) | 8.28 | 8.27 | 8.22 | 11.16 | 11.20 | 11.14 | 13.74 | 13.62 | 13.65 |
| R ($C_{ipso}$-$C_{ortho}$) | 1.41 | 1.42 | 1.42 | 1.41 | 1.42 | 1.42 | 1.41 | 1.42 | 1.41 |
| R ($C_{ipso}$-$C_{ipso}$) | 1.42 | 1.41 | 1.41 | 1.42 | 1.41 | 1.41 | 1.42 | 1.42 | 1.42 |
| R ($C_{ortho}$-$C_{ortho}$) | 1.40 | 1.40 | 1.42 | 1.40 | 1.40 | 1.40 | 1.40 | 1.40 | 1.40 |
| R ($C_{ipso}$-$C'_{ipso}$) | 1.50 | 1.49 | 1.48 | 1.49 | 1.48 | 1.48 | 1.49 | 1.48 | 1.48 |

The strain energies for the [n]CPY nanorings, that is, the energy released upon linearization of the cyclic nanoring, has been calculated by devising an appropriate homodesmotic reaction[37]

$$\Delta H_{strain}\ ([n]CPY) = \Delta H_f^0\ ([n]CPY) - n\left[\Delta H_f^0\ (bipyrene) - \Delta H_f^0\ (pyrene)\right] \qquad (1)$$

where $\Delta H^0_f$([n]CPY), $\Delta H^0_f$(bipyrene) and $\Delta H^0_f$(pyrene) are the enthalpy of formation at 0 ºK (i. e. with the zero-point vibrational energy included) of optimized [n]CPY, bipyrene and pyrene molecules, respectively, according to the scheme 1. Table 2 collects the calculated strain energies for [n]CPY and for their corresponding [2n]CPP.[37] As it was expected, the cyclic structures with pyrene units, i.e. [n]CPY, shows higher values for strain energies than their analogous [2n]CPP, although following the same trend found before for [2n]CPP values, i.e. the larger the system is, the lower strain energy becomes (see figure S1 in the supporting material). This fact might be related with a less favored synthesis due to higher structural and/or steric difficulties. Note that the strain energy of [4]CPY calculated before,[21] at the B3LYP/6-31G* level and thus without considering non-covalent interactions, is close to the value obtained in this work, although not completely similar due to the introduction here of intra-molecular non-covalent interactions.

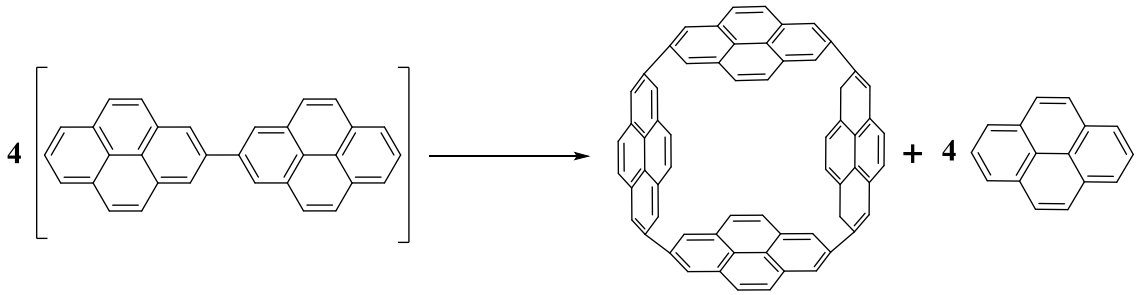


**Scheme 1.** Homodesmotic reaction used to determine the strain energy for [4]CPY taken as example.

**Table 2**. **Evolution of strain energy, $\Delta H_{strain}$ (in kcal/mol), and HOMO-LUMO energy difference, $\Delta E_{HOMO\text{-}LUMO}$ (in eV), for the [n]CPY systems and for their corresponding [2n]CPP compounds, calculated at the B3LYP-D3(BJ)/cc-pVDZ level**.

| | $\Delta H_{strain}$ | $\Delta E_{HOMO\text{-}LUMO}$ | | $\Delta H_{strain}$ | $\Delta E_{HOMO\text{-}LUMO}$ |
|---|---|---|---|---|---|
| [3]CPY | 112.50 | 3.06 | [6]CPP[b] | 89.83 | 3.07 |
| [4]CPY | 85.65 (93.69)[a] | 3.41 (3.48)[a] | [8]CPP[b] | 67.77 | 3.35 |
| [5]CPY | 72.72 | 3.48 | [10]CPP[b] | 54.25 | 3.49 |

[a] Values taken from reference [21]

[b] Values taken from reference [37]

Figure 3 shows the energy and shape of the fully delocalized HOMO and LUMO orbitals for the [n]CPY systems and the pyrene monomer. Similarly to strain energies, when the size of the system increases, the HOMO

energy decreases, while the LUMO energy increases, which produces, obviously, a larger HOMO-LUMO energy difference with the system size (see also table 2). Moreover, if we compare the HOMO-LUMO energy difference of [n]CPY and [2n]CPP, system by system, we find very similar values, with a marginal difference of only 0.06 eV between [4]CPY and [8]CPP, which could indicate a similar response after irradiation of samples.

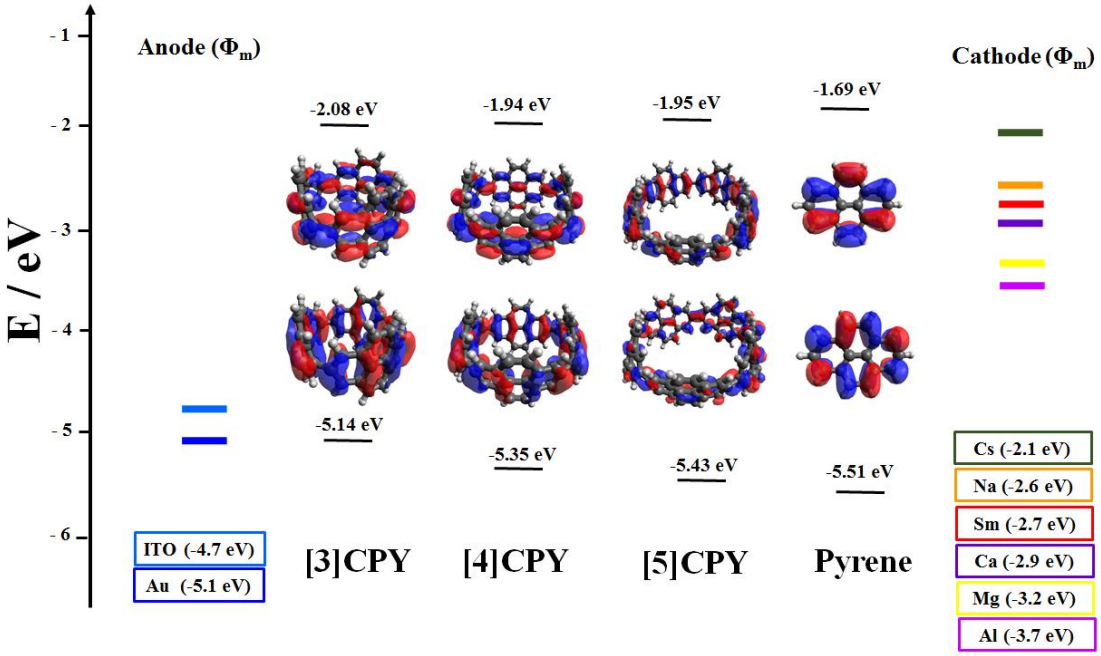


**Figure 3**. Isocontour plots (0.02 a.u.) and energy values of HOMO and LUMO orbitals for [n]CPYs and pyrene, calculated at the B3LYP-D3(BJ)/cc-pVDZ level, and the work function of the most useful electrodes used in opto-electronic devices.

To conclude the part of the study dealing with the properties of isolated nanorings, the UV-Vis absorption spectra has also been computed at the TD-PBE0/cc-pVDZ level using the Polarizable Continuum Model (PCM), with the default technical parameters and using chloroform as solvent, at the previously solvated (in chloroform) re-optimized structures at the B3LYP-D3(BJ)/cc-pVDZ level. Table 3 gathers the main component of low-energy electronic transitions for which the oscillator strength is found large enough, while figure S2 (see Supporting Information) shows the theoretically simulated UV-Vis absorption spectra for [3-5]CPY systems. Note that the HOMO to LUMO transition is symmetry forbidden in all the studied [n]CPY systems, which has also been observed for their analogous [2n]CPP, being thus involved in the transitions another set of low-lying molecular orbitals. Moreover, a red-shifting is observed in the series [3]CPY to [5]CPY, with a gradual decrease in the oscillator strength value. For [4]CPY, a good agreement between theoretical and experimental values has been observed, with a difference of only 0.03 eV (see table 3).

**Table 3. Main electronic transition energies (E, in eV) and oscillator strength (f) values for the [n]CPY structures, calculated at the TD-PBE0/cc-pVDZ//B3LYP-D3(BJ)/cc-pVDZ level, using chloroform as solvent.**

| Compound | E | f | Main Component of the transition (% contribution) |
|---|---|---|---|
| [3]CPY | 4.13 | 1.7903 | HOMO-4 → LUMO (27.8%)<br>HOMO-2 → LUMO+3 (28.9%) |
| | 4.13 | 1.7939 | HOMO → LUMO+4 (22.7%)<br>HOMO-5 → LUMO (22.8%)<br>HOMO-1 → LUMO+3 (28.8%)<br>HOMO → LUMO+5 (22.8%) |
| [4]CPY | 4.02 | 1.2952 | HOMO-3 → LUMO+4 (21.6%)<br>HOMO-2 → LUMO+4 (21.6%) |
| | 4.02 | 1.2955 | HOMO-3 → LUMO+4 (21.6%)<br>HOMO-2 → LUMO+4 (21.6%) |
| | 3.99[a] | experimental | |
| [5]CPY | 3.78 | 0.8677 | HOMO-6 → LUMO (17.2%)<br>HOMO-5 → LUMO (15.8%) |
| | 3.91 | 1.0048 | HOMO-5 → LUMO+3 (22.9%)<br>HOMO-4 → LUMO+5 (14.1%)<br>HOMO → LUMO+6 (13.9%) |

[a] Values taken from reference [21]

**Supramolecular issues: the case of [4]CPY.** The unique (and then different) dimer arrangements of [4]CPY have been extracted from its crystalline form, and used rigidly herein. Due to the fact that dihydro[4]CPY is the only compound with a fully resolved crystal structure,[21] we have consequently removed the solvent molecules (occluded into the cavity of the nanoring) and unsaturated correspondingly the molecule. The intermolecular interaction energy of every extracted dimer, $\Delta E_{int}$, depends on the geometrical arrangements of the isolated monomers to form the dimers at the crystal structure, and it has been calculated by subtracting the energy of both monomers at the dimer geometry ($G^{crystal}$) from that of the dimer[38]

$$\Delta E_{int} = Edimer\ (G^{crystal}) - [E_{monomer1}(G^{crystal}) + E_{monomer2}(G^{crystal})] \quad (2)$$

with negative values implying that the dimer structure is stabilized by weak (i.e. non-covalent) interactions.

By using these calculated $\Delta E_{int}$ values it is possible to estimate the cohesive or lattice energy, *U*, of the crystal, which usually is defined as the amount of energy required to separate a mole of the solid into the gas of its constituent molecules,[38] and obtained by using the following equation

$$U = -\frac{1}{2}\sum_i m_i \Delta E_{int}^{(i)} \quad (3)$$

where $m_i$ is the number of unique pairs extracted from the crystal structure in which it is possible to decompose it, and $\Delta E_{int}^{(i)}$ is the interaction energy for each dimer *i* calculated by using the equation (2). This value must be divided by two to avoid the double-counting of these energies,[39] and can be further related to the sublimation enthalpy ($\Delta_s H$) at room temperature (298.15 K) by $U = \Delta_s H\ (T) + 2RT$, being 2RT the classical thermal contribution.

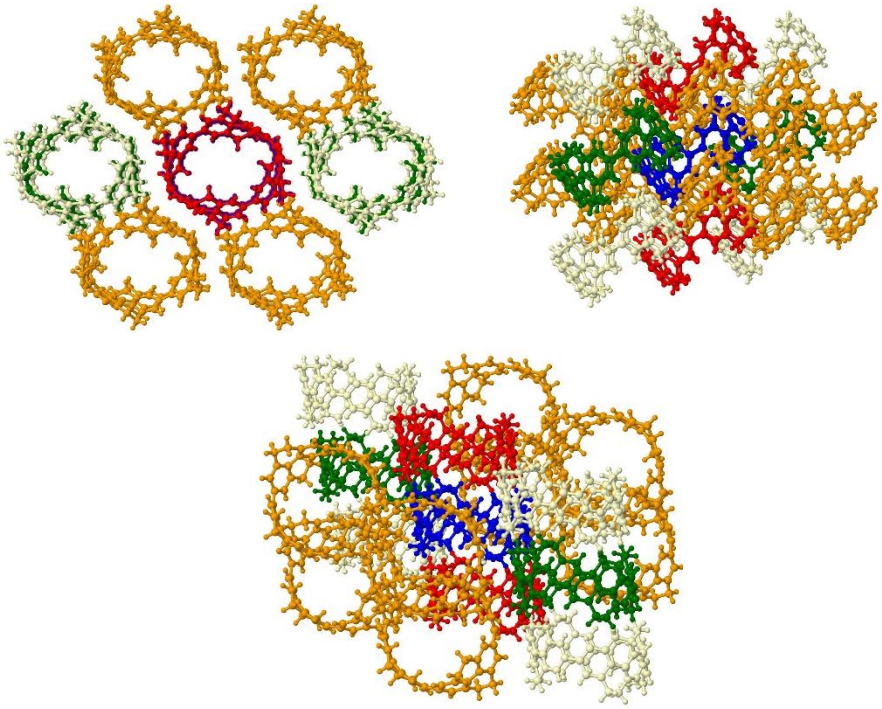

**Figure 4.** Supramolecular arrangement of dihydro[4]CPP in the crystalline state, from which the different dimers for interaction and cohesive energies have been extracted. The reference molecule, from which the number of uniquely symmetry-interacting dimers is determined, is blue-coloured. The different views correspond to the three crystallographic directions considered.

Figure 4 shows the supercell structure for the dihydro[4]CPY crystal, which was used to extract the different dimers to determine the cohesive energy. The packing of this molecule follows a herringbone-like pattern in which one may observe *parallel* dimers (i.e. two adjacent molecules - blue / green - belonging to the same layer and interacting along both in-plane directions of the crystal), *herringbone* dimers (i.e. two molecules - blue / orange - belonging to different, but not superimposed, layers) and *homotubular* dimer (i.e. two adjacent - blue / red - and superimposed molecules belonging to two different layers and interacting along the vertical axis). In that sense, the crystalline structure of the recently synthesized dihydro[4]CPY nanoring comprises the set of unique dimers displayed in figure 5, with their calculated interaction energies gathered in Table 4. We have employed here a set of increasingly large basis set, from the 6-31G** (moderate) to the cc-pVTZ (large), to estimate (and then reduce) the associated BSSE in these calculations. Table 4 also shows the associated cohesive energy obtained from this crystal structure. The values for interaction energies are ranging from -10.25 to -21.77; -9.53 to -20.27 and -8.71 to -17.63 kcal/mol, calculated with the 6-31G**, cc-pVDZ and cc-pVTZ basis sets, respectively. Independently of the basis set size, the lowest value has always been obtained for the parallel dimer, while the highest interaction energies are those for homotubular dimers. The corresponding B3LYP-D3(BJ)/cc-VTZ interactions energies for the dimers of [8]CPP were found similar. The only difference has been observed for the parallel dimer, whose value is now the lowest for [4]CPY while, for [8]CPP, situates indeed between the extremes. Interestingly, no large difference for these interaction energies is found with respect to the dimers of [8]CPP, ranging from -0.8 kcal/mol (from the herringbone-1 dimer and its corresponding analogue) up to -3.6 kcal/mol (for homotubular dimers and its corresponding analogue), respectively. On the other hand, the homotubular arrangement also yields the highest interaction energy for [4]CPY, as it happened too for the [8]CPP case. The greatest stability found for the homotubular dimers could be related with the preferred crystalline growth of the self-assembled samples.

**Table 4. Interaction energies (kcal/mol) for the different [4]CPY dimers and the associated cohesive energy, calculated at different levels of theory.**

| | B3LYP-D3(BJ) | | |
|---|---|---|---|
| | 6-31G** | cc-pVDZ | cc-pVTZ |
| Parallel | -10.25 | -9.53 | -8.71 |
| Herringbone-1 | -11.67 | -10.96 | -9.88 |
| Herringbone-2 | -11.70 | -10.97 | -9.88 |
| Herringbone-3 | -13.90 | -12.80 | -11.51 |
| Herringbone-4 | -13.90 | -12.80 | -11.51 |
| Homotubular | -21.77 | -20.27 | -17.63 |
| Cohesive Energy | 83.22 | 77.33 | 69.11 |

The cohesive energy of [4]CPY has been further estimated from the interaction energies calculated above. This estimation allows us to compare it with other similar systems such as polycyclic aromatic hydrocarbons (PAHs), and/or to determine the relative contribution of each of the dimers to the cohesive energy. Moreover, as we can infer from figure 4, all the dimers contribute in the same degree (i.e., there are two dimers for each disposition) to the calculated cohesive energy. The obtained cohesive energy values, *U*, for the [4]CPY structure are 83.22, 77.33 and 69.11 kcal/mol, calculated with the 6-31G**, cc-pVDZ and cc-pVTZ basis set, respectively. Note also the large BSEE associated to the widely used 6-31G** basis set, compared with the nearly-converged cc-pVTZ basis set. Comparing with the [8]CPP at the same level of theory[38] by using the same methodology, the value for [4]CPY is significantly higher than that obtained for its analogous [8]CPP (i.e. 45.96 kcal/mol at the B3LYP-D3(BJ)/cc-pVTZ level). It is also possible to estimate theoretically the sublimation enthalpy by applying an approximate expression such as $\Delta H_s = 4.162 + 6.185\ C_{aromatic}$ (in kJ/mol, and where $C_{aromatic}$ is the number of C atoms involved in aromatic systems).[38] Therefore, [4]CPY and [8]CPP, with molecular formulae $C_{64}H_{32}$ and $C_{48}H_{32}$, would yield values as high as *U* = 96.8 kcal/mol and *U* = 72.54 kcal/mol, respectively, and thus severely overestimated with respect to the ones calculated here from first-principles. However, for pyrene and bipyrene, the latter way of calculating *U* leads to values of 24.65 and 48.30 kcal/mol, respectively, and, thus, close to the experimental value (24.14 kcal/mol) in the case of pyrene.[40] This discrepancy reflects once more the key role played by the cyclic topology of [n]CPY compounds, as the source of the differences found here with respect to theoretical predictions based on linear-regression of data extracted from more standard compounds.

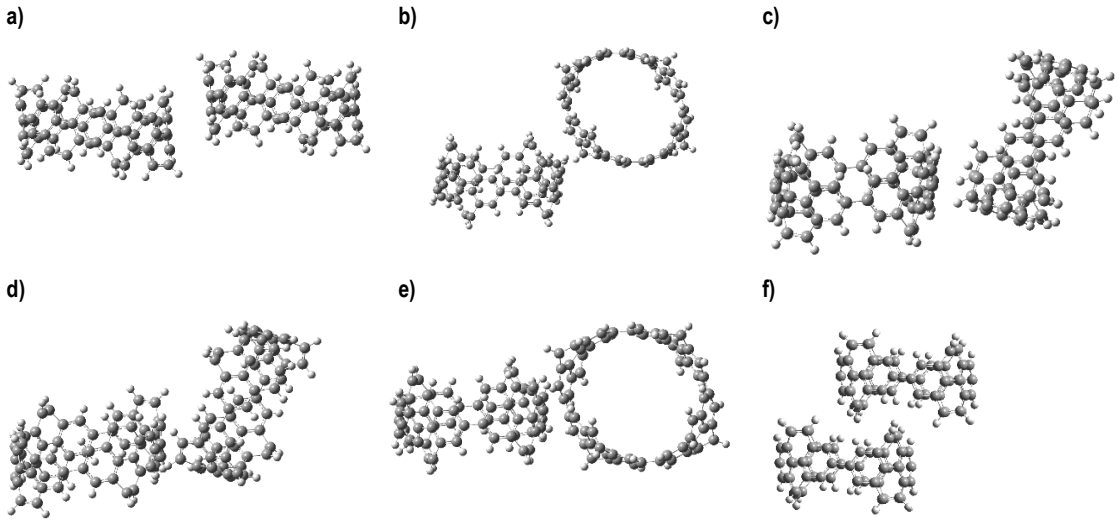


**Figure 5.** Sketch of the different dimers found for [4]CPY being labelled as a) parallel; b) herringbone-1; c) herringbone-2; d) herringbone-3; e) herringbone-4; f) homotubular, respectively.

**Semiconducting properties of [n]CPY.**

Theoretical Framework. A high performance of organic molecular semiconductors in optoelectronic devices relies on an efficient charge injection from electrodes and sufficiently high charge mobilities within the active layer of the device. In typical π-conjugated organic (crystalline) materials with small bandwidths (< 1eV) at room temperature, the charge diffusion across the samples is generally described by a hopping mechanism,[41,42] where the lattice vibrations and the coupling with the charge carriers (i.e. the molecular packing as well the conformation of a single molecule) control the transport efficiency.[43] In the zero-limit, that is, at high temperature and according to the Marcus-Levich-Jortner (MLJ) model,[44,45] the charge-transport rate $k_{CT}$ for a self-exchange charge-transfer (CT) reaction between neighboring molecules, can be expressed as

$$k_{CT} = \frac{4\pi^2}{h} V_{if}^2 \sqrt{\frac{1}{4\pi\lambda_s k_B T}} \sum_{n=0}^{\infty} \left[ exp\left(-S_{eff}^n\right) \times \frac{S_{eff}^n}{n!} \times exp\left( \frac{-\left(\lambda_s + n\hbar\omega_{eff} + \Delta G^0\right)^2}{4\lambda_s k_B T} \right) \right] \quad (4)$$

depending, mainly, on the charge transfer integral or electronic coupling ($V_{if}$) and the classical contribution ($\lambda_s$), mostly the external, to the reorganization energy fixed here at 0.1 eV, according to common practice within the field. Generally, in organic crystals the outer contribution is of the order of few tenths of an electronvolt, contrarily to charge transfer in solution wherein the external part dominates.[46-50] ΔG° is the Gibbs energy difference between the electronic states involved in the charge-transfer process (equal to zero in the self-exchange process), $S_{eff} = \lambda_i/\hbar\omega_{eff}$ is the effective Huang−Rhys factor, where $\lambda_i$ is the inner reorganization energy, and $\omega_{eff}$ is the frequency of the effective vibrational mode assisting the process, fixed here at $\hbar\omega_{eff} \sim 0.2$ eV. Note that, $\lambda_i$ must be as low as possible, while $V_{if}$ must be maximized in order to improve the charge transport.

The inner reorganization energy, $\lambda_i$, for self-exchange consists of two terms ($\lambda_i = \lambda_1 + \lambda_2$) corresponding to the geometry relaxation energies going from the neutral-state geometry to the charged-state one and *vice versa* (Nelsen four-point method)[51,52]

$$\lambda_1 = E^0(G^*) - E^0(G^0) \quad (5)$$

$$\lambda_2 = E^*(G^0) - E^*(G^*) \quad (6)$$

where $E^0(G^0)$ and $E^*(G^*)$ are the ground-state energies of the neutral and ionic states, respectively, $E^0(G^*)$ is the energy of the neutral molecule at the optimized ionic geometry and $E^*(G^0)$ is the energy of the charged molecule at the optimized neutral geometry.[46,50,53,54] Additionally, from this set of calculations, it is possible to extract also the values of adiabatic ionization potential (AIP) or adiabatic electron affinity (AEA) as the difference of total energies between charged and neutral systems

$$AIP = E^*(G^*) - E^0(G^0) \;//\; AEA = E^0(G^0) - E^*(G^*) \quad (7)$$

While their corresponding vertical (V) energies are calculated as

$$VEA\ (VIP) = AEA\ (AIP) + \lambda_2 \quad (8)$$

Note that, $V_{if}$ describes the electronic coupling between two neighboring molecules,[46,50] and, hence, it critically depends on their relative spatial arrangement and is given by the matrix element $V_{if} = \langle\Psi_i|\hat{H}|\Psi_f\rangle$, where $\hat{H}$ is the electronic Hamiltonian of the system. The wave functions of the initial, $\Psi_i$, and final, $\Psi_f$, charge-localized states are normally obtained in the hypothetical absence of any coupling between the molecular units.[41,53,55] However, we have determined $V_{if}$ values as one-half of the energy difference between the adiabatic potential energies at the geometry ($G_c$) where the diabatic (localized) potential energy surfaces cross each other.[56,57]

$$V_{if} = \frac{1}{2}\left[E_+(G) - E_-(G)\right]_{G=G_c} \quad (9)$$

This two-state model involves the solution of the equation

$$\begin{vmatrix} H_{ii} - E & H_{ij} - ES_{if} \\ H_{fi} - ES_{fi} & H_{ff} - E \end{vmatrix} = 0 \quad (10)$$

From which

$$V_{if} = \frac{1}{1 - S_{if}^2} \left[ H_{if} - \frac{S_{if}\,(H_{ii} + H_{ff})}{2} \right] \quad (11)$$

with $S_{if} = \langle \Psi_i | \Psi_f \rangle$, $H_{if} = \langle \Psi_i | \hat{H} | \Psi_f \rangle$, $H_{ii} = \langle \Psi_i | \hat{H} | \Psi_i \rangle$ and similarly $H_{ff}$. We have used the unrestricted Hartree-Fock (UHF) wave function ( $\Psi_f$, being f = i, j) to describe the excess charge (both, hole and electron) localized on the initial and final states for a hole or electron transfer reaction. Note that this excess charge has been checked to remain completely localized on one (and only one) of the molecules during the set of calculations performed. This way of estimating electronic coupling values has recently been benchmarked for acene-based organic semiconductors, with very successful results.[58]

To achieve a good charge injection, the frontier MOs and the work-function ($\Phi_m$) of the electrode must have appropriately close values. An ohmic contact is produced when the energy difference between the frontier MO and $\Phi_m$ is equal or lower than 0.3 eV. In the case of *p*-type semiconductors, the HOMO must be aligned with the Fermi levels of environmentally stable anodes, such as ITO[59] to obtain an efficient hole injection. By contrast, in the case of *n*-type semiconductors, the LUMO should match the Fermi level of electrodes with low work function, such as Na, Cs, Ca, Mg, Ba or Al.[60] Although this is actually an approximation, i.e. interface dipole effects between electrode and semiconductor are not taken into account,[61,62] the comparison of $\Phi_m$ with HOMO/LUMO energy levels of the semiconductor may help to determine whether charge injection is likely or, on the contrary, if a high contact resistance should be expected. These dipoles came from either partial charge-transfer metal-semiconductor, the reduction of the metal work function by the organic layer or the occupation of the metal-induced density of states in the gap of the organic material.[63,64] As a result, the gap between semiconductor affinity and ionization levels at the metal/organic interface narrows up to several electronvolts as compared to the gas-phase frontier energy levels.[65,66] Any model aimed at a complete description of the metal/organic interface should account for those specific interactions. Accordingly, despite the fact that the free metal work function and the (gas-phase) HOMO/LUMO levels do not give the exact information, they serve as a qualitative guide for the electron/hole barrier injection and thus to establish trends within a set of related compounds.[63] Moreover, the values of the HOMO and LUMO orbitals must range between -4.8 / -5.5 eV and -3.6 / -4.5 eV, respectively, to improve the stability of the opto-electronic device.[45] However, some studies establish the limit value for the LUMO energy in -4.0 eV due to the fact that negative charges can react with atmospheric species such as water or oxygen.[67,68]

Ionization potentials (IP) and electron affinities (EA) are also key parameters that determine the efficiency of the charge injection from the electrodes and the susceptibility to be reduced or oxidized upon air exposure.[54] Thus, the EA of a semiconductor must be ≥ 3.0 eV for an easy electron injection, but not much greater than 4.0 eV to avoid destabilization under ambient conditions.[47] Low IPs facilitate hole injection but too low values can produce unintentional doping. As we stated before, we have finally studied the semiconductor nature of the selected [n]CPY, through their charge injection and transport inside of the material.

Charge Injection. The EA and IP (both, adiabatic and vertical) values for holes and electrons, upon increasing the size of the systems, are shown in table 5, which also collects the values for the corresponding [2n]CPP analogues. We remind that to inject an electron into the LUMO level of the molecule, the EA (defined as the energy released when

one electron is added to the system in the gaseous state) must be high enough, to ensure the efficient charge injection and improve the environmental stability of the material (although these considerations are not a general guideline for predicting the air stability); while IP (defined as the energy released when one electron is removed to the system in the gaseous state) must be low enough to allow an efficient hole injection into the HOMO level. The small difference in the vertical and adiabatic values indicates that the structural relaxation upon charge injection is small. We have observed that the VIP values reach form 6.136 eV (for [3]CPY) to 6.207 eV (for [4]CPY), without following any sequence according to the size of the ring. However, AEA values increase with size (from 1.086 to 1.213 eV). The small AEA values indicates that the [n]CPY might have a large barrier for electron injection, showing their radical anions a low stability at room atmosphere. In that sense, some investigations have showed that the AEA values should be greater than 2.8 eV for air-stable n-channel materials due to the inherent instability of organic anions in air[47,69] thus, the low AEA could jeopardize the stability of the studied compounds. On the other hand, the low values of AIP indicate that the hole injection seems to be favored following the sequence [4]CPY > [5]CPY > [3]CPY. Comparing the AEs and IPs for [n]CPY with their analogous values for [2n]CPP,[70] the introduction of pyrene rings decrease the EAs values, which might indicate a high instability in the radical anions, observing the same trend for IPs values.

**Table 5**. **Intramolecular electron ($\lambda_i^-$) and hole ($\lambda_i^+$) reorganization energies, adiabatic (AEA) and vertical (VEA) electron affinities and adiabatic (AIP) and vertical (VIP) ionization potentials calculated at the B3LYP-D3(BJ)/cc-pVDZ level, for the [n]CPY systems and their corresponding [2n]CPP compounds. All magnitudes are given in eV.**

| Compounds | AEA | VEA | $\lambda_i^-$ | AIP | VIP | $\lambda_i^+$ | $\lambda_i^-$ / $\lambda_i^+$ ratio |
|---|---|---|---|---|---|---|---|
| [3]CPY | 1.086 | 0.995 | 0.185 | 6.136 | 6.230 | 0.193 | 0.96 |
| [4]CPY | 1.131 | 1.010 | 0.221 | 6.207 | 6.284 | 0.165 | 1.34 |
| [5]CPY | 1.213 | 1.147 | 0.138 | 6.174 | 6.239 | 0.126 | 1.09 |
| | | | | | | | |
| [6]CPP[a] | 1.287 | 1.101 | 0.373 | 6.194 | 6.382 | 0.380 | 0.98 |
| [8]CPP[a] | 1.294 | 1.142 | 0.302 | 6.237 | 6.379 | 0.281 | 1.07 |
| [10]CPP[a] | 1.323 | 1.191 | 0.266 | 6.235 | 6.340 | 0.231 | 1.15 |

[a] Values taken from reference [70]

Following with the study of the frontier molecular orbitals (see figure 2), we had observed how HOMO eigenvalues decreased with increasing *n*, which indicates a stabilization of the systems. However, for LUMO energy orbitals, this behavior is not observed, with close values for all the systems. At this stage, and regarding the gap between orbital energy values and their difference with respect to the electrode work function, it is possible to determine, from a qualitative point of view, the ability of hole and electron injection and, concomitantly, determine the redox stability of organic semiconductors. In that sense, the smallest difference between HOMO and LUMO orbitals can be related with the easiness of charge injection. Comparing the HOMO-LUMO gap of [n]CPY and their analogous [2n]CPP, the obtained values are similar with a difference ranging between 0.01 and 0.06 eV. In both cases ([n]CPY and [2n]CPP) the lowest gap has been calculated for n = 3, which might enhance to the conductivity efficiency, because they could use electrodes with narrow work function. On the other hand, comparing the HOMO/LUMO level with the work function of some widely used electrodes, we can predict an ohmic contact for electron injection ($|E_{LUMO} - \Phi_m| <$ 0.3 eV) for all [n]CPY compounds with Cs electrode ($\Phi_m$ = 2.14 eV); while an ohmic contact for hole injection is predicted with Au ($\Phi_m$ = 5.1 eV) and ITO ($\Phi_m$ = 4.7 eV) electrodes, also, for all the studied [n]CPY systems (see also figure 3).

Charge transport estimates. Table 5 also shows the values of internal reorganization energy of the [n]CPY systems and their [2n]CPP analogues. As we can observe, the internal reorganization energies $\lambda_i$ previously reported for the

series of [2n]CPP compounds are, approximately, in the range of 0.35 – 0.20 eV and 0.47 – 0.20 eV for hole and electron transport, respectively, with their values smoothly decreasing with the increasing number of *n*. These obtained $\lambda_i$ values are higher than those obtained for some state-of-the-art systems which have been used in the fabrication of opto-electronic devices.[31,71] However, the substitution of CPP by CPY rings produces a marked decrease in $\lambda_i$, ranging now from 0.126 / 0.193 eV and 0.138 / 0.221 eV for hole and electron transport, respectively. These later values are closer to the range of other typical *n*-type compounds such as anthracene,[31] perfluorepentacene,[72] while the $\lambda_i$ values for hole transport are similar or even lower than those found for tetratiofulvene derivatives,[73] or some oligoacenes[74] and oligothiophenes,[75] antracene or tetracene,[76] which are known to behave as efficient *p*-type semiconductors in OFETs. In a first approximation, using these values to determine the ambipolar character of [n]CPY compounds and their related [2n]CPP, we observe that the introduction of pyrene rings changes only slightly the ambipolar behavior expected for the [2n]CPP analogues. In that sense, [3]CPY ([6]CPP) and [5]CPY ([10]CPP]) show similar performance, which might anticipate an ambipolar behavior of active layers composed of these materials. However, in the case of [4]CPY (and the [8]CPP), the hole transport seems to be slightly preferred.

On the other hand, the calculated electronic coupling values and their associated charge transfer rates for the different dimers of [4]CPY (see figure 5) are included in table 6. From the obtained $V_{if}$ values, we can extract some conclusions: (i) the $V_{if}$ values calculated for electron are higher than those for hole, except for the herringbone-4 arrangement, whose electron $V_{if}$ value is negligible; ii) for hole transport, the $V_{if}$ value obtained for the herringbone-4 arrangement is the highest for all cases, and thus with an expectedly large contribution to the whole hole charge-transport rate; iii) for electron transport, the $V_{if}$ value electron calculated from the homotubular arrangement yields now the highest value. Actually, the calculated $V_{if}$ values are in the range of those obtained before for state-of-the-art molecules such as naphathalene, anthracene, tetracene, pentacene or rubicene molecules.[50] As a consequence of the interplay between reorganization energies and electronic couplings, see equation (4), the total electron (hole) charge-transport rate reaches values as high as $2.7 \times 10^{13}$ $s^{-1}$ ($5.5 \times 10^{12}$ $s^{-1}$). Overall, the hole charge-transport rate reaches values higher than for the corresponding electron charge-transport rate, being the hole transport clearly favored by a 5-fold factor.

**Table 6. Estimates hole and electron electron coupling ($V_{if}$, in meV) and the corresponding charge transfer rate ($k_{CT}$, in $s^{-1}$) for the referred dimers of the [4]CPY, calculated at the UHF/cc-pVDZ level.**

| | Holes | | Electrons | |
|---|---|---|---|---|
| | $V_{if}$ | $k_{CT}$ | $V_{if}$ | $k_{CT}$ |
| Parallel | 0.012 | $1.27 \times 10^{6}$ | 0.185 | $2.84 \times 10^{8}$ |
| Herringbone-1 | 0.268 | $6.34 \times 10^{8}$ | 0.509 | $1.73 \times 10^{9}$ |
| Herringbone-2 | 0.025 | $6.51 \times 10^{6}$ | 2.26 | $3.41 \times 10^{10}$ |
| Herringbone-3 | 0.091 | $7.31 \times 10^{7}$ | 0.241 | $3.88 \times 10^{8}$ |
| Herringbone-4 | 55.3 | $2.70 \times 10^{13}$ | 0.001 | $6.67 \times 10^{3}$ |
| Homotubular | 6.88 | $4.18 \times 10^{11}$ | 28.6 | $5.47 \times 10^{12}$ |

## CONCLUSION

In this work, we have studied the influence of the increasing number of pyrene rings in the properties of the recently synthetized cyclic Cyclo-2,7-PYrenylene (CPY) nanorings, ranging from geometrical (some selected bond lengths and the diameter of the nanoring), structural (strain energies and other properties derived from crystalline packing such as the cohesive energy), and electronic (such as electronic transition energies and the study of the charge injection and associated mobility inside of the material).

We have systematically calculated some selected bond lengths of neutral and charged nanorings, observing how the size and/or the electronic state of the [n]CPY systems do not significantly alter the values. The diameter of the inner cavity linearly increases, as it was expected, with the system size. On the other hand, the strain energy decreases with the size of [n]CPY systems, in order to minimize the steric hindrance, created upon self-cyclation, concomitantly observing an increase in the HOMO-LUMO gap with the size of the nanoring, which situates between 3 – 3.5 eV according to the system size. Additionally, the absolute values of the frontier molecular orbital might align favorably with the work function of some widely used electrodes, and thus promote an efficient charge (hole or electron) injection.

The supramolecular properties for [4]CPY, such as interaction energies for the different dimers (extracted of the crystal structure) and the associated cohesive energy, have been also analyzed. The calculated value of the cohesive energy shows a sufficiently high stabilization by weak (non-covalent) interactions, although lower than that expected for the corresponding linear oligomer; thus indicating the key role played by the cyclic topology of these compounds, in agreement with recent studies on the other nanohoops also acting as nanotube segments.

Finally, we have also calculated the charge-transport rate for [4]CPY, after obtaining the electronic coupling values for all the dimers extracted from crystalline data. The compounds present a balanced charge-transport rate, that is displaying values for hole-transport are slightly higher than for electron-transport, which might anticipate the efficient use of these nanorings in field-induced applications.

## SUPPORTING INFORMATION AVAILABLE

(S1) Evolution of strain energies for [n]CPY and [2n]CPP as a function of the system size (n). (S2) Theoretically simulated UV-Vis spectra for [n]CPY compounds, calculated at the TD-PBE0/cc-pVDZ//B3LYP-D3(BJ)/cc-pVDZ level using chloroform as solvent.

## ACKNOWLEDGEMENTS

This work is supported by the ``Ministerio de Economía y Competitividad'' of Spain and the ``European Regional Development Fund'' through project CTQ2014-55073-P

## REFERENCES

[1] Omachi, H.; Nakayama, T.; Takahashi, E.; Segawa, Y.; Itami, K. Initiation of Carbon Nanotube Growth by Well-Defined Carbon Nanorings. *Nat. Chem.,* **2013**, *5,* 572–576.

[2] Tahara, K.; Tobe. Y. Molecular Loops and Belts. *Chem. Rev.,* **2006,** *106*, 5274–5290

[3] Darzi, E. R.; Jasti, R. The Dynamic, Size-Dependent Properties of [5]-[12]Cycloparaphenylenes. *Chem. Soc. Rev.,* **2015**, *44*, 6401–6410.

[4] Lewis, S. E. Cycloparaphenylenes and Related Nanohoops. *Chem. Soc. Rev.,* **2015**, *44*, 2221–2304.

[5] Segawa, Y.; Yagi, A.; Matsui, K.; Itami, K. Design and Synthesis of Carbon Nanotube Segments. *Angew. Chem. Int. Ed.,* **2016**, *55*, 5136–5158.

[6] Yagi, A.; Segawa, Y.; Itami, K. Synthesis and Properties of [9]Cyclo-1,4-Naphthylene: A π-extended Carbon Nanoring. *J. Am. Chem. Soc.,* **2012**, *13*, 2962–2965

[7] Batson, J.; Swager, T. M. Towards a Perylene-Containing Nanohoops. *Synlett.* **2013**, *24*, 2545 – 2549.

[8] Zhang, B.; Manning, G. P.; Dobrowloski, M. A.; Cyrański, M. K.; Bodwell, G. J. Nonplanar Aromatic Compunds. 9. Synthesis, Structure and Aromaticity of 1:2,13:14-Dibenzo[2]paracyclo[2](2,7)-pyrenophane-1,13-diene. *Org. Lett.* **2008**, *10*, 273–276;

[9] Yagi, A.; Venkataramana, G.; Segawa, Y.; Itami, K. Synthesis and Properties of Cycloparaphenylene-2,7-Pyrenylene: A Pyrene-Containing Carbon Nanoring. *Chem. Commun.,* **2014**, *50,* 957–959.

[10] Hitosugi, S.; Nakanishi, W.; Yamasaki, T.; Isobe, H. Bottom-up Synthesis of Finite Models of Helical (*n,*m)-Single-Wall Carbon Nanotubes. *Nat. Commun.,* **2011**, *2*, 492–495.

[11] Matsuno, T.; Kamata, S.; Hitosugi, S.; Isobe, H. Bottom-up Synthesis and Structures of π-Lengthened Tubular Macrocyles. *Chem. Sci.,* **2013**, *4*, 3179–3183.

[12] Kammermeier, S.; Jones, P. G.; Herges, R. Ring-Expanding Metathesis of Tetradehydro-anthracene – Synthesis and Structure of a Tubelike, Fully Conjugated Hydrocarbon. *Angew. Chem. Int. Ed.,* **1996**, *35*, 2669–2671.

[13] Machón, M.; Reich, S.; Maultzsch, J.; Okudera, H.; Simon, A.; Herges, R.; Thomsen, C. Structural, Electronic and, Vibrational Properties of (4,4)Picotube Crystals. *Phys. Rev. B: Condens. Matter. Mater. Phys.,* **2005**, *72*, 155402.

[14] Matsui, K.; Segawa, Y.; Itami, K. Synthesis and Properties of Cycloparaphenylene-2,5-pyridylidene: A Nitrogen-Containing Carbon Nanoring. *Org. Lett.,* **2012**, *14*, 1888–1891.

[15] Darzi, E. R.; Hirst, E. S.; Weber, C. D.; Zakharov, L. N.; Lonergan, M. C.; Jasti, R. Synthesis, Properties, and Design Principles of Donor-Acceptor Nanohoops. *ACS Cent. Sci.,* **2015**, *1*, 335–342.

[16] Ito, H.; Mitamura, Y.; Segawa, Y.; Itami, K. Thiophene-Based, Radical π-Conjugation: Synthesis, Structure, and Photophysical Properties of Cyclo-1,4-phenylene-2',5'-thienylenes. *Angew. Chem. Int. Ed.,* **2015**, *54,* 159–163.

[17] Thakellapalli, H.; Farajidizaji, B.; Butcher, T. W.; Akhmedov, N. G.; Popp, B. W.; Petersen, J. L.; Wang, K. K. Syntheses and Structures of Thiophene-Containing Cycloparaphenylenes and Related Nanohoops. *Org. Lett.,* **2015***, 17*, 3470–3473.

[18] Kuwabara, T.; Orii, J.; Segawa, Y.; Itami, K. Curved Oligophenylenes as Donor in Shape-Persistent Donor-Acceptor Macrocycles with Solvatofluorochromic Properties. *Angew. Chem. Int. Ed.,* **2015**, *54*, 9646–9649.

[19] Myśliwiec, K.; Kondratowicz, M.; Lis, T.; Chmielewski, P. J.; Stępień, M. Highly Strained NonClassical Nanotube End-caps. A Single-Step Solution Synthesis from Strain-Free, Non-Macrocyclic Precursors. *J. Am. Chem. Soc.,* **2015**, *137*, 1643–1649.

[20] Ball, M.; Fowler, B.; Li, P.; Joyce, L. A.; Li, F.; Liu, T.; Paley, D.; Zhong, Y.; Li, H.; Xiao, S.; Ng. F.; Steigerwald, M. L.; Nuckolls, C. Chiral Conjugated Corrals. *J. Am. Chem. Soc.,* **2015***, 137*, 9982–9987.

[21] Iwamoto. T.; Kayahara, E.; Yasuda, N.; Suzuki, T.; Yamago, S. Synthesis, Characterization and Properties of [4]Cyclo-2,7-pyrenylene: Effects of Cyclic Structure on the Electronic Properties of Pyrene Oligomers. *Angew. Chem. Int. Ed.,* **2014**, *53*, 6430–6434.

[22] Bodwell, G. J.; Miller, D. O.; Vermeij, R. J. Nonplanar Aromatic Compounds. 6. [2]Paracyclo[2](2,7)pyrenophane. A Novel Strained Cyclophane and a First Step on the Road of a "Vögtle" Belt. *Org. Lett.,* **2001**, *3*, 2093–2096.

[23] Figueira-Duarte, T. M.; Müllen, K. Pyrene-Based Materials for Organic Electronics. *Chem. Rev.,* **2011**, *111*, 7260–7314.

[24] Frisch, M. J.; Trucks, G. W.; Schlegel, H. B.; Scuseria, G. E.; Robb, M. A.; Cheeseman, J. R.; Scalmani, G.; Barone, V.; Mennucci, B.; Petersson, G.A.; *et al.* Gaussian 09, revision D.01; Gaussian Inc.: Wallingford, CT, **2009**.

[25] Valiev, M.; Bylaska, E. J.; Govind, N.; Kowalski, K.; Straatsma, T. P.; Van Dam, H. J.; Wang, D.; Nieplocha, J.; Apra, E.; Windus, T.; *et al.* NWChem: A Comprehensive and Scalable Open-Source Solution for Large Scale Molecular Simulation. *Comput. Phys. Commun.,* **2010**, *181,* 1477–1489.

[26] Becke, A. D. Density-Functional Thermochemistry. III. The Role of Exact Exchange. *J. Chem. Phys*. **1993**, *98*, 5648–5652;

[27] Lee, C.; Yang, W.; Parr, R. G. Development of the Colle-Salvetti Correlation-Energy Formula into a Functional of the Electron Density. *Phys. Rev. B*. **1988**, *37*, 785.

[28] Hung, Y. C.; Jiang, J. C.; Chao, C. Y.; Su, W. F.; Lin, S. T. Theoretical Study on the Correlation Between Band Gap, Bandwidth, and Oscillator Strength in Fluorene-Based Donor-Acceptor Conjugated Copolymers. *J. Phys. Chem. B.*, **2009**, *113*, 8268–8277.

[29] Lin, B. C.; Cheng, C. P.; Lao, Z. P. M. Reorganization Energies in the Transport of Holes and Electrons in Organic Amines in Organic Electroluminiscence Studies by Density Functional Theory. *J. Phys. Chem. A*, **2003**, *107*, 5241–5251.

[30] Randic, M. Aromaticity of Polycyclic Conjugated Hydrocarbons. *Chem. Rev.,* **2003**, *103*, 3449–3606.

[31] Coropceanu, V.; Malagoli, M.; da Silva Filho, D. A.; Gruhn, N. E.; Bill, T. G.; Brédas, J. L. Hole- and Electron-Vibrational Coupling in Oligoacene Crystal: Intramolecular Contributions. *Phys. Rev. Lett*., **2002**, *89,* 275503−275507

[32] Grimme, S.; Antony, J.; Ehrlich, S.; Krieg, H. A Consistent and Accurate *Ab Initio* Parametrization of Density Functional Theory Correction (DFT-D) for the 94 Elements H-Pu. *J. Chem. Phys.,* **2011**, *132*, 154104.

[33] Grimme, S.; Ehrlich, S.; Goerigk, L. Effect of the Damping Function in Dispersion Corrected Density Functional Theory. *J. Comput. Chem.,* **2011**, *32*, 1456–1465.

[34] Grimme, S.; Hansen, A.; Brandenburg, J. G.; Bannwarth, C. Dispersion-Corrected Mean-Field Electronic Structure Methods. *Chem. Rev.,* **2016**, *116*, 5105–5154.

[35] Jacquemin, D.; Perpète, E. A.; Coifini, I.; Adamo, C. Accurate Simulation of Optical Properties in Dyes. *Acc. Chem. Res*. 2009, **42**, 326–334.

[36] Perdew, J. P.; Burke, K.; Ernzerhof, M. Generalized Gradient Approximation Made Simple. *Phys. Rev. Lett*., **1996**, *77*, 3865.

[37] Climent-Medina, J. V.; Pérez-Jiménez, A. J.; Moral, M.; San-Fabián, E.; Sancho-García, J. C. Intra- and Intermolecular Dispersion Interaction in [*n*]Cycloparaphenylenes: Do They influence Their Structural and Electronic Properties?. *ChemPhysChem.,* **2015**, *16*, 1520–1528.

[38] Reche-Tamayo, M.; Moral, M.; Pérez-Jiménez, A.J.; Sancho-García, J.C. Theoretical Determination of Binding and Cohesive Energies of Weakly Bound Cycloparaphenylene Molecules. *J. Phys. Chem. C.,* **2016**, submitted for publication.

[39] Schweizer, W. B.; Dunitz, J. B. Quantum Mechanical Calculations for Benzene Dimer Energies: Present Problems and Future Challenges. *J. Chem. Theory Comput.,* **2006**, *2*, 288–291.

[40] Roux, M. V.; Temprado, M. Chickos, J. S.; Nagano, Y. Critically Evaluated Thermochemical Properties of Polycyclic Aromatic Hydrocarbons. *J. Phys. Chem. Ref. Data,* **2007**, *37*, 1855–1996.

[41] Wang, L.; Nan, G.; Yang, X.; Peng, Q.; Li, Q.; Shuai, Z. Computational Methods for Design of Organic Materials with High Charge Mobility. *Chem. Soc. Rev*., **2010**, *39*, 423–434.

[42] Chen, X-K.; Zou, L-Y.; Huang, S.; Min, C-G.; Ren, A-M.; Feng, J-K.; Sun, C-C. Theoretical Investigation of Charge Injection and Transport Properties of Novel Semiconductor Materials-Cyclic Oligothiophenes. *Org. Electron*., **2011,** *12*, 1198–1210.

[43] Duhm, S.; Xin, Q.; Hosoumi, S.; Fukagawa, H.; Sato, K.; Ueno, N.; Kera, S. Charge Reorganization Energy and Small Polaron Binding Energy of Rubrene Thin Fillm by Ultraviolet Photoelectron Spectroscopy. *Adv. Mater.,* **2012**, *24,* 901–905.

[44] Marcus, R. A. Electron Transfer Reaction in Chemistry. Theory and Experiment. *Rev. Mod. Phys*. **1993,** *65*, 599.

[45] Barbara, P. F.; Meyer, T. J.; Ratner, M. A. Contemporary Issues in Electron Transfer Research. *J. Phys. Chem*., **1996,** *100*, 13148–13168.

[46] Brédas, J. L.; Beljonne, D.; Coropceanu, V.; Cornil, J. Charge-Transfer and Energy-Transfer Processes in π-Conjugated Oligomers and Polymers: A Molecule Picture. *Chem. Rev*., **2004**, *104*, 4971–5004.

[47] Newman, C. R.; Frisbie, C. D.; da Silva Filho, D. A.; Brédas, J. L.; Ewbank, P. C.; Mann, R. K. Introduction to Organic Thin Film Transistors and Design of n-Channel Organic Semiconductors. *Chem. Mater*., **2004***, 16,* 4436–4451.

[48] Troisi, A. Charge Transport in High Mobility Molecular Semiconductors: Classical Models and New Theories. *Chem. Soc. Rev*., **2011**, *40*, 2347–2358.

[49] Coropceanu, V.; André, J. M.; Malagoli, M.; Brédas, J. L. The Role of Vibronic Interaction of Intramolecular and Intermolecular Electron Transfer in π-Conjugated Oligomers. *Theor. Chem. Acc*., **2003**, *110*, 59–69.

[50] Coropceanu, V.; Cornil, J.; da Silva Filho, D. A.; Olivier, Y.; Silbey, R.; Brédas, J. L. Charge Transport in Organic Semiconductors. *Chem. Rev*., **2007**, *107*, 926–952.

[51] Nelsen, S. F.; Blackstock, S. C.; Kim, Y. Estimation of Inner Shell Marcus Terms for Amino Nitrogen Compounds by Molecular Orbital Calculations. *J. Am. Chem. Soc*., **1987**, *109*, 677–682.

[52] Nelsen, S. F.; Yunta, M. J. R. Estimation of Marcus λ for p-Phenylenediamines from The Optical Spectrum of a Dimeric Derivative. J. *Phys. Org. Chem*., **1994**, *7*, 55–62.

[53] Cheung, D. L.; Troisi, A. Modelling Charge Transport in Organic Semiconductors: From Quantum Dynamics to Soft Matter. *Phys. Chem. Chem. Phys*., **2008**, *10*, 5941–5952.

[54] Sancho-García, J. C. Application of Double-Hybrid Density Functional to Charge Transfer in N-Substituted Pentacenequinones. *J. Chem. Phys*. **2012**, *136*, 174703.

[55] Moral, M.; García, G.; Garzón, A.; Granadino-Roldán, J. M.; Fernández-Gómez, M. DFT Study of the Effect of Fluorine Atoms on the Crystal Structure and Semiconducting Properties of Poly(Arylene-Ethynylene) Derivatives. *J. Chem. Phys.,* **2016**, *144*, 154902

[56] Newton, M. D. Quantum Chemical Probes of Electron-Transfer Kinetics: The Nature of Donor-Acceptor Interactions. *Chem. Rev.,* **1991**, *91*, 767–792.

[57] Farazdel, A.; Dupuis, M.; Clementi, E.; Aviram, A. Electric-Field Induced Intramolecular Electron Transfer in Spiro. Pi. – Electron Systems and Their Suitability as Molecular Electronic Devices. A Theoretical Study. *J. Am. Chem. Soc.,* **1990**, *112*, 4206–4214.

[58] Thorley, K. J.; Risko, C. Mapping the Configuration Dependence of Electronic Coupling in Organic Semiconductors. *J. Mat. Chem. C.,* **2016**, *4*, 3825–3832.

[59] Sun, S. S.; Dalton, L. R. Introduction to Organic Electronic and Optoelectronic Materials and Devices; CRC Press: Taylor & Francis Group, New York, **2005.**

[60] Michaelson, H. B. The Work Function of the Elements and Its Perioricity. *J. Appl. Phys*., **1977**, *48*, 4729.

[61] McMahon, D. P.; Troisi, A. Evaluation of the External Reorganization Energy of Polyacenes. *J. Phys. Chem. Lett.,* **2010**, *1*, 941–946.

[62] Körzdörfer, T.; Parrish, R. M.; Sears, J. S.; Sherrill, C. D.; Brédas, J. L. On the Relationship Between Bond-Length Alternation and Many-Electron Self-Interaction Error. *J. Chem. Phys.* **2012**, *137*, 124305–124313.

[63] Cheng, X.; Noh, Y. Y.; Wang, J.; Tello, M.; Frisch, J.; Blum, R. P.; Vollmer, A.; Rabe, J. P.; Koch, N. T.; Sirringhaus, H. Controlling Electron and Hole Charge Injection in Ambipolar Organic Field-Effect Transistors by Self-Assembled Monolayers. *Adv. Funct. Mater.,* **2009**, *19*, 2407–2415.

[64] Amy, F.; Chan, C.; Kahn, A. Polarization at the Gold/Pentacene Interface. *Org. Electron.,* **2005**, *6*, 85–91.

[65] Natali, D.; Caironi, M. Charge Injection in Solution-Processed Organic Field-Effect Transistors: Physics, models and Characterization Methods. *Adv. Mater.,* **2012**, *24*, 1357–1387.

[66] Crispin, X.; Geskin, V.; Crispin, A.; Cornil, J.; Lazzaroni, R.; Salaneck, W. R.; Brédas, J. L. Characterization of The Interface Dipole at Organic/Metal Interface. *J. Am. Chem. Soc.,* **2002**, *124*, 8131–8141.

[67] Anthopoulos, T. D.; Anyfantis, G. C.; Papavassiliou, G. C.; de Leeuw, D. M. Air-Stable Ambipolar Transistors. *Appl. Phys. Lett.,* **2007**, *90*, 122105.

[68] Zhan, X.; Facchetti, A.; Barlow, S.; Marks, T. J.; Ratner, M. A.; Wasielewski, M. R.; Marder, S. R. Rylene and Related Diimides for Organic Semiconductors. *Adv. Mater*., **2011**, *23*, 268–284.

[69] Chang, Y. C.; Kuo, M. Y.; Chen, C. P.; Lu, H. F.; Chao, I. On the Air Stability of *n*-Channel Organic Field-Effect Transistors: A Theoretical Study of Adiabatic Electron Affinities of Organic Semiconductors. *J. Phys. Chem. C.,* **2010**, *114*, 11595–11601.

[70] Sancho-García, J.C.; Moral, M.; Pérez-Jiménez, A.J. Effect of Cyclic Topololgy on Charge-Transfer Properties of Organic Molecular Semiconductofs: The Case of Cycloparaphenylene. *J. Phys. Chem. C.,* **201**6*, 120*, 9104–9111.

[71] McGarry, K. A.; Xie, W.; Sutton, C.; Risko, C.; Wu, Y.; Young, W. G.; Brédas, J. L.; Frisbie, C. D.; Douglas. C. J. Rubrene-Based Single-Crytal Organic Semiconductor: Synthesis, Electronic Structure and Charge-Transport Properties. *Chem. Mater.,* **2013**, *25*, 2254–2263.

[72] Kera, S.; Hosoumi, S.; Sato, K.; Fukagawa, H.; Nagamatsu, S.; Sakamoto, Y.; Suzuki, T.; Huang, H.; Chen, W.; Wee, A. T. S.; Corpoceanu, V.; Ueno, N. Experimental Reorganization Energies of Pentacene and Perfluoropentacene: Effects of Perfluorination. *J. Phys. Chem. C.,* **2013**, *117*, 22428–22437.

[73] Otón, F.; Pfattner, R.; Pavlica, E.; Olivier, Y.; Moreno, E.; Puigdollers, J.; Bratina, G.; Cornil, J.; Fontronoda, X.; Mas-Torrent, M. *et al.* Electron-Withdrawing Substituted Tetrathiafulvalenes as Ambipolar Semiconductors. *Chem. Mater.,* **2011**, *23*, 851–861.

[74] Deng, W-Q.; Goddard III, W.A. Predictions of Hole Mobilities in Oligoacene Organic Semiconductors from Quantum Mechanical Calculations. *J. Phys. Chem. B.,* **2004**, *108*, 8614–8621.

[75] Sokolov, A. N.; Atahan-Evrenk, S.; Mondal, R.; Akkerman, H. B.; Carrera-Sánchez, R. S.; Granados-Focil, S.; Schrier, J.; Mannsfeld, S. C. B.; Zoombelt, A. P.; Bao, Z.; Aspuru-Guzik, A. From Computational Discovery to Experimental Characterization of a High Hole Mobility Organic Crystal. *Nature Commun.,* **2011**, *437*, 1–8.

[76] Cornil, J.; Brédas, J. L.; Zaumseil, J.; Sirringhaus, H. Ambipolar Transport in Organic Conjugated Materials. *Adv. Mater.,* **2007**, *19*, 1791–1799.